2
Cryomicroscopy

Frank Booy and **Elena Orlova**

Imperial College London, London, UK

2.1 The need for (electron) microscopy

A light microscope extends the range of the eye, enabling visualization of objects otherwise too small to be seen. Ultimately its resolving power is limited to $\sim$1 μm by the wavelength of the light used. This means that we can see a bacterium but not a virus particle. To extend the eye's range further we must use radiation of not only a shorter wavelength but also a type for which we can make a focussing device (lens) to form an image. X-rays have a shorter wavelength (e.g. Cu $K_\alpha \approx$ 1.5 Å) but no simple lens is available. Electrons are charged particles (waves); at 100 kV their wavelength is 0.037 Å and in a magnetic or electric field they experience a force and can thus be focussed. Therefore an electron microscope (EM) is simply a microscope that uses electrons instead of light. The first such microscope was developed by Ruska in the 1930s (Nobel Laureate 1986), but its widespread application and development was delayed by the second World War. In fact further technological development was required before it was to become useful for examining frozen, hydrated specimens.

2.2 Development of cryomicroscopy

Cryo-electron microscopy did not come of age until the 1980s, after the development of differential pumping permitted film to be separated from the frozen sample by a factor of 100 or so in vacuum in the microscope, improved anti-contamination systems prevented the sample itself acting as a cold trap and stable specimen cooling

Chemical Biology Edited by Banafshé Larijani, Colin. A. Rosser and Rudiger Woscholski

holders became available. Gatan developed the most widely used routine side-entry cooling holder. Siemens developed the ultimate holder with stability achieved by cooling the complete specimen and objective lens assembly to 4 K using liquid helium. As a consequence the lens became superconducting. Unfortunately Siemens closed their electron optical division and it was left to the Berlin group (under Zeitler) with Philips (now FEI) to develop this into a fully functional cryo-EM (due largely to the dedication of Zeitler and Zemlin). This functioned beautifully until retirement closed the group in 1997. The microscope has now been moved to Goettingen, Germany. Fujiyoshi and collaborators in Japan developed a very stable, top-entry (and thus fixed-tilt) cryo-EM in the 1990s running at liquid helium temperature (4 K) (now marketed by Jeol), and FEI developed a eucentric, helium-cooled cryo-EM. These are the more common top-end cryo-EMs of today, capable of atomic resolution augmented by their use of 200–300 kV and field emission guns.

A modern electron microscope is capable of $\sim$1 Å resolution and is shown schematically in Figure 2.1. It consists of a source of electrons, a number of lenses,

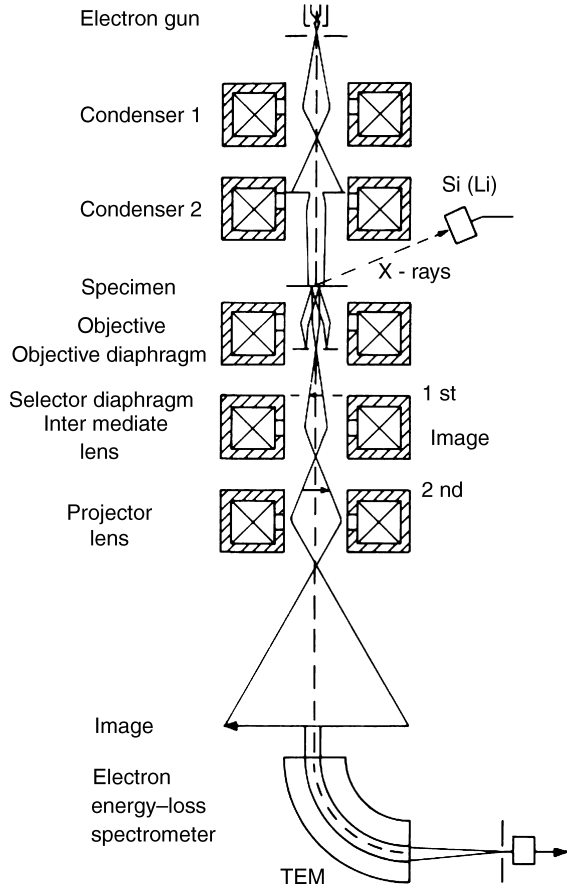

Figure 2.1 Schematic diagram of an electron microscope with X-ray detector and post column energy filter. [Reproduced from Hawkes (2004)]

a viewing screen and a data collection system. The simplest electron source is a heated tungsten filament. When electrons have energy greater than the work function of tungsten, they escape and form a pool of free electrons that may be accelerated in an electric field. If a crystal, commonly LaB_6, is attached to the filament, electrons may be induced to emit from a single crystal face and emerge with greater coherence and current density from a smaller, effective source. A further improvement occurs when the electrons are extracted by field emission from a tungsten crystal, and this is the source of choice for cryo-EM. The tip may either be cold or partially heated (Schottky emission). The electrons are then accelerated through voltages typically of 100–300 kV when they are travelling at relativistic speeds ($\sim c/2$ at 100 kV). The convergence and energy density of the electron beam are controlled by two condensor lenses prior to interaction with the specimen. The objective lens is the contrast-forming lens with an aperture in its back focal plane and provides a basic increase in magnification ($\times$20–50). The image formed by this lens is subsequently magnified by a further series of intermediate and projector lenses before the electrons impinge on a fluorescent viewing screen, CCD (charge-coupled device) camera detector or sheet of film. It is also possible to image the back focal plane of the objective lens, thus forming an electron diffraction pattern.

2.3 Sample–electron interaction

Electrons have a large scattering cross section compared with, say, X-rays and interact very strongly with matter. For this reason an electron microscope has to be maintained under vacuum and only dry samples can be investigated. This has serious consequences for biological materials, which comprise typically some 85 per cent water. Thus tremendous effort has gone into developing methods for supporting samples as they are dehydrated prior to observation. Methods involving chemical cross-linking and staining ultimately distort the native structure and thus limit the details visualized and the resolution obtained. Sucrose, glucose, trehalose or tannic acid have been used to stabilize/replace bound water both at room temperature and in the frozen, hydrated state. However, water is unique and nothing can replace it without introducing potentially significant, structural changes. An alternative approach to dehydration was suggested by Fernandes-Moran, namely to look at samples maintained in a frozen state inside the microscope. At a low enough temperature, the vapour pressure of water is sufficiently small for the sample to retain its water. The viability of cryo-EM was demonstrated by Chanzy in Europe and Glaesar and Taylor in the USA in the 1970s, where electron diffraction experiments showed that freezing could preserve high-resolution structure in hydrated polysaccharide and protein crystals. Also in the 1970s, Parsons developed an environmental cell in which the sample was maintained at room temperature in a fully hydrated state and he was able to demonstrate high-resolution structural preservation by electron diffraction. However, a consequence of the strong interaction of electrons is that the thickness of the sample that may be investigated is limited and thus the wet cell, with its associated water vapour, was impractical for imaging.

Electrons may be scattered elastically (with no loss of energy) or inelastically (with loss of energy). Inelastically scattered electrons are not brought into focus by the objective lens in the same plane as elastically scattered electrons. They can, however, provide useful information about the atomic make-up of the sample in energy loss spectroscopy. With 100 kV electrons the mean free path in ice (the average distance the electron travels before interaction) is ~1000 Å. For an interpretable image this is an indication of appropriate maximum specimen thickness. This increases for more energetic electrons at higher accelerating voltages. Typically, as the thickness of the sample increases, the resolution that can be achieved decreases due to plural and inelastic scattering. For these reasons high-resolution studies by cryo-electron microscopy have been limited to thinner samples. The use of an energy filter to remove inelastically scattered electrons from the image does enable somewhat thicker samples to be investigated and is currently important in tomographic studies. However, thicker samples, such as whole cells, must be first sectioned or fractured before microscopy, and their treatment is beyond the scope of this chapter.

2.4 Contrast in negatively stained and cryo preparations

Prior to the advent of cryo-EM, the standard method for examining smaller specimens was negative staining, first introduced by Ruska in 1937. Indeed, staining remains the simplest method for specimen observation to ~20 Å. In this technique the sample is dried down in a pool of a heavy metal salt (typically uranyl acetate) that supports the structure and maps out its surface features. Strong image contrast results from the scattering difference between the heavy metal surrounding the structure and the protein, which is seen as a light object in a darker background.

The basic idea of cryo EM is very simple and is illustrated in Figure 2.2. A drop of the specimen of interest is applied to a continuous or holey or lacey carbon film on an EM grid, reduced in thickness by blotting with filter paper and then plunged into liquid ethane maintained close to its freezing point by liquid ethane. Supercooling takes place at some 10^4–10^6 °C/s resulting in vitrification of a thin specimen in the μs to ms time range. Excess ethane is then blotted off and the grid is transferred into a specimen cooling holder for examination and photography close to liquid nitrogen temperature. Refinements to freezing equipment now permit the control of parameters such as humidity and temperature prior to freezing, automated, reproducible blotting and the release of caged molecules or spraying of molecules to induce defined changes just prior to freezing.

Because the sample is chemically untreated it is acutely sensitive and susceptible to damage by the beam of ionizing radiation (much as we would be!) and must be imaged under the lowest dose conditions that are compatible with an acceptable signal-to-noise ratio. To a first approximation, the scattering of electrons is proportional to the density of the material. Thus a protein, with a density of ~1.3, is seen as a darker object in the less dense aqueous background (density ~0.95 for ice), which means that the contrast has been reversed as compared with visualization in negative stain. Figure 2.3 shows T4 phage as an example. The contrast obtained is low and normally enhanced by defocusing the objective lens.

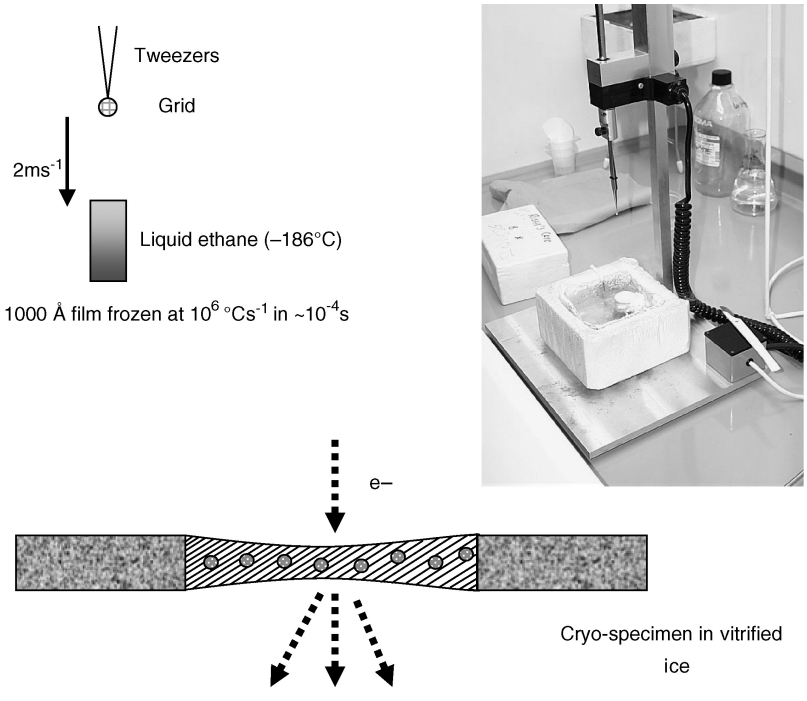

Figure 2.2 Left: schematic diagram to show that plunging a grid at 2 m/s into liquid ethane cooled by liquid nitrogen achieves a vitreous state for a 1000 Å layer in the ms to μs time frame with surface cooling rates $\sim 10^6\,^{\circ}\mathrm{Cs}^{-1}$. Right: traditional freezing equipment. Below: schematic diagram of vitreous sample spanning a hole in a grid in the EM

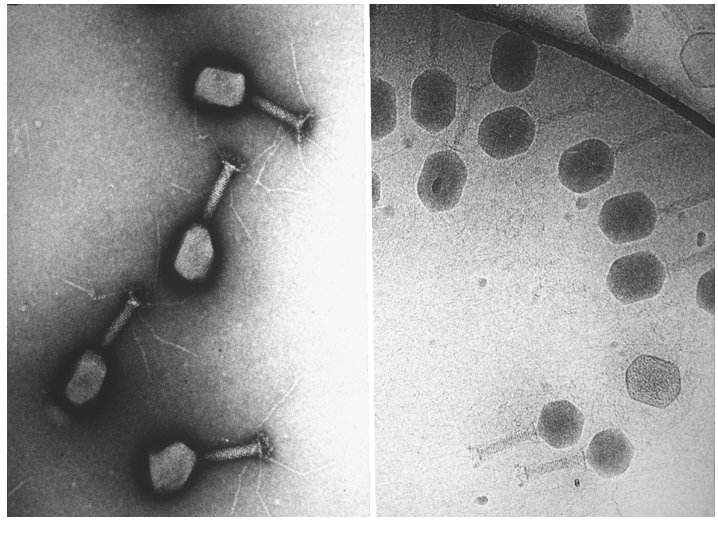

Figure 2.3 The appearance of T4 phage after negative staining with uranyl acetate (a) and in the frozen, hydrated state (b). Note the reversal of contrast between (a) and (b) [Micrograph (a) is courtesy of Dr Naiqian Cheng]

2.5 Image formation

Electron microscopes are able to provide images at very high magnification. There is, however, a trade-off between high and low magnification. A microscope is designed to give its optimum electron-optical performance at high magnification but the electron dose (for the same optical density on the film) depends on the magnification squared. It is thus of acute interest to know at how low a magnification a particular EM will still provide atomic resolution. Often the limitation is a stray magnetic field. A further complication is that the images obtained do not provide a direct representation of the specimen spatial density distribution. The contrast results from the scattering differences between the protein and water modified by the properties of the objective lens. Image contrast arises from two components: amplitude and phase. Amplitude contrast results from absorption or strong scattering of the incident beam by the sample with the scattered electrons removed from the image by the objective aperture. For a thin cryo specimen the amplitude contrast has been estimated at 7 per cent. Phase contrast results from interference of elastically scattered electrons with the unscattered beam; the amplitude of the scattered wave is unaffected. It is as if the object were transparent. Such thin, unstained, biological samples that only scatter electrons through small angles are often described as 'weak phase objects'. Additional phase contrast is generally introduced by defocusing the objective lens when spherical aberration enhances the contrast of images further. A more detailed description of image formation can be found in Reimer (1997). The visualization of weak phase objects by defocusing results in considerable complexity in interpreting the image as a simple projection of the specimen. This arises because image details in a particular size-range may be present in the image with different contrast, even complete contrast reversal. Many years of analysis have resulted in the development of specialized software to restore the original density distribution of images. This is referred to as correction of the contrast transfer function of the EM (or simply CTF correction). After this correction, the image of the weak phase object can be considered as a true two-dimensional projection of the three-dimensional object. This permits the use of special mathematical approaches to obtain a complete three-dimensional density distribution for the object.

2.6 Image analysis

The development of specialist software for the analysis of electron micrographs has equipped researchers with a variety of computational tools to analyse different types of sample. These methods are all based on the premise that a micrograph is a simple projection of the object and therefore have much in common. The main steps include (i) pre-processing of images, (ii) restoration of images, (iii) enhancement of images, (iv) determination of orientations and (v) reconstruction of the three-dimensional distribution of density. The result obtained must then be validated and interpreted.

Pre-processing is a set of operations designed to transform the data into the format required for the software, to determine the defocus at which the micrograph was

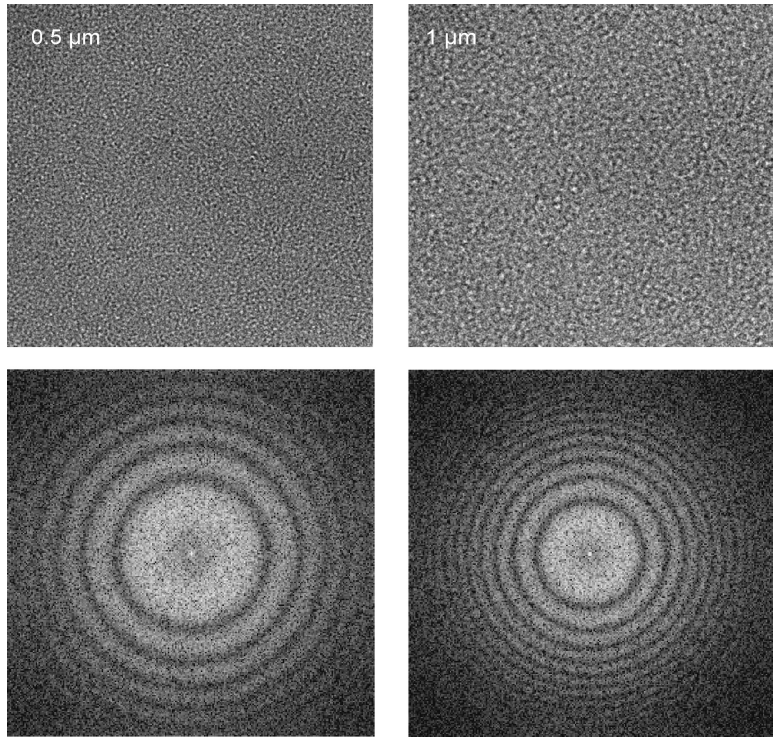

Figure 2.4 Images of a carbon film (taken at 200 kV on an FEI T-20 FEG-EM) at the defocus values indicated and their corresponding Fourier transforms. The light and dark bands are Thon rings which result from the contrast transfer function imposed by the objective lens of the microscope

taken and to normalize the data. Band pass filtering is usually applied to remove any uneven background and unimportant high-frequency detail.

The *restoration* step aims to restore the frequency spectrum of the image. Before the more common availability of electron microscopes equipped with a field emission gun, few image details were present in micrographs beyond the first Thon ring and this step was less important. Today, a typical high-quality, cryo-micrograph might have a first zero of the CTF at ~18 Å and information present to 6–10 Å in subsequent Thon rings (see Figure 2.4). To analyse such data beyond the first Thon ring requires careful correction of the CTF. In the most basic approach, this is achieved by simply reversing the phase of each odd Thon ring; a more complete approach requires additional correction of the amplitudes. This modifies the contrast of image details so that the image then reliably represents a true projection of the three-dimensional object and may be used to generate a more faithful reconstruction.

Enhancement is the procedure used to increase the signal-to-noise (S/N) ratio of images by averaging. For all types of specimen, there will be local variations in the thickness of the ice film, in concentration of the buffer salts and other contaminants and impurities such as denatured proteins. Random noise variation also arises from the support film and the effects of radiation damage on the ensemble. If

micrographs are recorded on film, the photographic emulsion will add shot noise; a CCD camera/photo multiplier also produces some additional noise. Although crystals and nonperiodic specimens are treated differently, the essence is simply averaging of similar particle images. For two-dimensional crystals averaging can be done using the Fourier spectrum of the crystal by extracting the periodic part of the spectrum and suppressing the background. The reverse Fourier transform then provides an average image in which the unit cell of the crystal is seen with an enhanced S/N ratio. For single particles, averaging is performed in real space, where the images are first aligned and then classified into different groups according to their various features. The assumption is made that the sample comprises identical subunits, each embedded with an arbitrary orientation in an ice film.

Determination of the orientations of different projections is an essential step prior to calculating a full three-dimensional map. In some cases, some information can be obtained during data collection, e.g. the tilt of the goniometer at which the images were recorded can be used initially in the tomographic analysis of two-dimensional crystals. For single particles the task is much more difficult. Today, there are two principal approaches, common lines and projection matching. The common lines approach is based on the fact that any two, 2-dimensional projections of a structure have at least one, 1-dimensional projection in common. Knowledge of the angles between these lines for at least three, 2-dimensional projections provides the necessary orientational parameters. The method was first used in reciprocal space by Crowther and later in real space by van Heel. In projection matching a comparison is made between the molecular images and all possible projections of the model. The orientation of the projection that has the closest similarity to the molecular image is assigned to the image. This approach is widely used in real space for particles with low symmetry and in Fourier space for particles with icosahedral symmetry.

In *reconstruction* of the three-dimensional distribution of molecular densities, there are two main approaches. The first is a real space approach and the second a Fourier space approach that is analogous to the crystallographic method. In real space, the 'back projection' technique is used to reverse the operation of obtaining a projection. A projection simply represents the total sum of all densities of the three-dimensional object in a single plane (somewhat like a medical X-ray). To restore the densities of the three-dimensional object the densities of the projections must be extended in the reverse of the projecting direction. There are several algorithms that perform this procedure.

The Fourier method is based on the central section theorem, which states that the Fourier transform of a projection is a central section in Fourier space. This means that projections at different angles then provide sections of Fourier space at these angles and thus the space can be filled up. We can thus obtain the complete three-dimensional Fourier transform of the object. The reverse Fourier transformation of such a volume will generate the three-dimensional density distribution of the object in real space. For particles with icosahedral or helical symmetry, a Fourier–Bessel transformation is widely used since the use of a cylindrical coordinate system may avoid some interpolation errors.

Validation and interpretation of the results obtained are necessary so that the quality of the reconstruction that has been obtained can be assessed. This can be

analysed computationally by estimating the size of the smallest detail that has been determined, i.e. the resolution, or more generally, by comparing the structure with all known structural and biochemical data. A general computational approach is to use the Fourier shell correlation (FSC). This is particularly useful when little additional information is available or the resolution is modest (e.g. 15 Å). For this, the data are divided randomly into two sets and two independent reconstructions and their Fourier transforms are calculated. Equivalent shells in Fourier space from each structure are compared and the spacing at which the correlation becomes poor provides an estimate of the resolution achieved. For higher resolution structures (say better than 10 Å), in addition to FSC analysis, one can potentially trace out α-helices at $\sim$8 Å and β-sheets at 6 Å or better. Parts of the structure that may be known already from X-ray or NMR studies can be fitted and an estimate of resolution made.

The structure of several large complexes consisting of a number of proteins has been determined by electron microscopy and their interpretation requires establishing the boundaries and linkages between the various fragments, some of whose structures are known from X-ray diffraction or NMR studies. This is known as docking or fitting of the atomic models into the EM map and is often used to validate the quality of the microscopy. Examples are shown in Figures 2.7–2.9.

The structures obtained must be *presented* in an understandable and convincing manner, which again means representation of a three-dimensional structure as two-dimensional pictures. Surface shadowing software provides an iso-surface representation. These are essentially snapshots of the structure as if it were illuminated by a distant light source. The threshold used for the surface shading should be chosen carefully to represent the expected mass of the protein, or within one σ above the average density of the structure. Alternatively, the data may be presented in the form of a series of simple density sections, which additionally provide insight into details of the internal structure. Figure 2.7 shows surface shaded and density section representations of reovirus.

2.7 Software used in the analysis of electron micrographs

There are many software packages written for the analysis of EM data. They can be divided into those used for preprocessing images and those enabling a complete analysis to a three-dimensional reconstruction. The former group includes software for the selection of particles from micrographs, sometimes in an automated manner, and software to determine the defocus and state of stigmation in order to carry out a CTF correction. With the current explosion towards higher resolution, such programs are rapidly evolving to optimize effectiveness and speed. ‘Ximdisp’ for the manual selection of particles is currently the most user friendly and reliable program that can be run in stand-alone mode, whose output is fully compatible with many other packages. A useful program just for CTF determination is CTFFIND3, which automatically determines defocus and stigmation parameters.

Packages that allow a complete analysis of images are well established but each package was originally developed for a specific group of specimens. The MRC

package was developed in the 1970s for the analysis of two-dimensional crystals and helices. With larger two-dimensional crystals it was possible to record electron diffraction patterns, which provided reliable amplitudes directly. In diffraction mode data are unaffected by specimen drift or the CTF of the microscope. Images of the crystals were used to derive phase information. To restore the complete three-dimensional distribution of amplitudes and phases in Fourier space, both electron diffraction and image data are required from several tilted specimens. This package permits the correction of lattice distortions (unbending), CTF correction, signal extraction from background noise, the merging of diffraction data recorded at different angles and calculation of the three-dimensional molecular density map.

Another group of packages analyses assemblies with helical symmetry. The first three-dimensional reconstruction method was developed for helical systems using a Fourier–Bessel approach. Today, the package Suprime is more commonly used and may be used to straighten filaments, analyse image spectra and perform three-dimensional analysis. However, some helical structures are very flexible and this results in changes in the helical parameters, i.e. disorder. Such difficulties are now being addressed using a single particle approach, where the helical assembly is cut into small elements that are analysed as single particles.

A number of packages relates to single particle analysis: these include the MRC package and its modified version Simplex, EM3DR, both of which are aimed at the analysis of structures with icosahedral or D5 symmetry. Many viruses display or enclose a capsid with icosahedral symmetry. Such structures may consist of one or several different proteins and vary in size from $\sim$200 to 2000 Å and are classified by a T number or a tiling approach. The icosahedral symmetry imposes a 60-fold degeneracy of information that permits the determination of a three-dimensional structure from just a few images. Most packages for the analysis of icosahedral structures use a Fourier–Bessel approach in contrast to other single particle packages, which use real space algorithms, primarily the back projection method. Packages such as IMAGIC-5, SPIDER, EMAN and Xmipp are used for analysis of single particle images with low or no symmetry. These packages utilise thousands of images of individual molecules. The software enables CTF correction, image alignment, orientation determination and the calculation of three-dimensional reconstructions.

Situs, URO, MOLREP, EMfit are packages that may be used for the *interpretation and objective fitting* of data. O and PyMOL are used mainly for manual fitting and inspection of data.

The software used to present results includes: surface representation (shading) Amira, Iris Explorer, PyMol, Chimera. Amira is an advanced software system for 3D visualization. Iris Explorer is powerful software that is particularly useful for surface shading and density interpretation. PyMOL is a molecular graphics system with an embedded script writer, and Python interpreter is, designed for real-time visualization and rapid generation of high-quality molecular graphics images and animations. It permits editing and fitting of PDB coordinates into three-dimensional maps. Chimera is an interactive molecular graphics program.

2.8 Examples

We have discussed the need for examining specimens close to their native state by cryo-EM and shown that high-resolution, but noisy, images result. After data analysis and image enhancement by computer processing, a three-dimensional reconstruction can be determined. We now present that state of the art with some of the highlights that have been achieved to date.

2.8.1 Two-dimensional crystals

These are assemblies of molecules that are organized crystallographically in two rather than three dimensions. They sometimes occur naturally, e.g. in bacterial membranes such as purple membrane or porin. For microscopy they are most easily interpreted when they are a just a single molecular layer thick. Considerable success has been achieved with membrane proteins. Their natural environment in the membrane permits detergent solubilization and subsequent crystallization in a lipid bilayer. Nonmembrane proteins may also form 2d crystals. Data are collected and analysed from samples tilted to $\pm 60^{\circ}$. Symmetry of the molecule and crystallographic symmetry are used to minimize the effect of the uneven distribution of Fourier sections. The latest reconstruction of halorhodopsin has been obtained at 5 Å resolution. Y. Fujiyoshi and colleagues were able to determine a density map of bacteriorhodopsin at 3.5 Å resolution (Figure 2.5)

2.8.2 Helical structures

These may be considered as two-dimensional crystals that have been rolled up to form a cylinder with the unit cells matching at the line of connection, which may

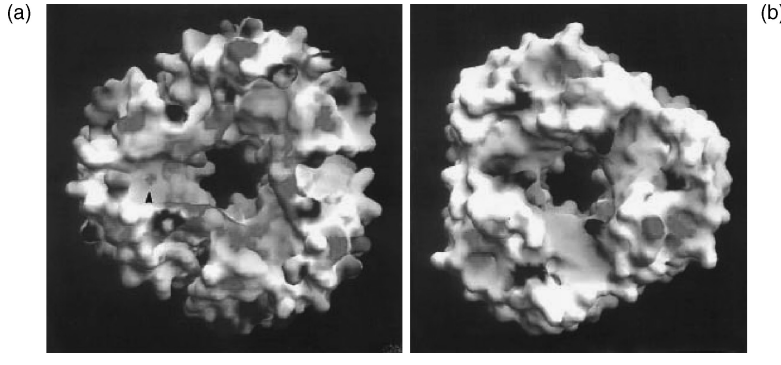

Figure 2.5 Illustration of a structure determined from analysis of 2D crystals at 3 Å resolution. Surface shaded views of (a) the cytoplasmic side and (b) the extracellular side of the bacteriorhodopsin trimer. Blue and red areas indicate positive and negative surface charges respectively. The arrow indicates the opening of the only proton channel that can be seen in this view. [Reproduced from Fujiyoshi, Y. (1999) *Faseb J.* **13** (suppl 2): S191–194]

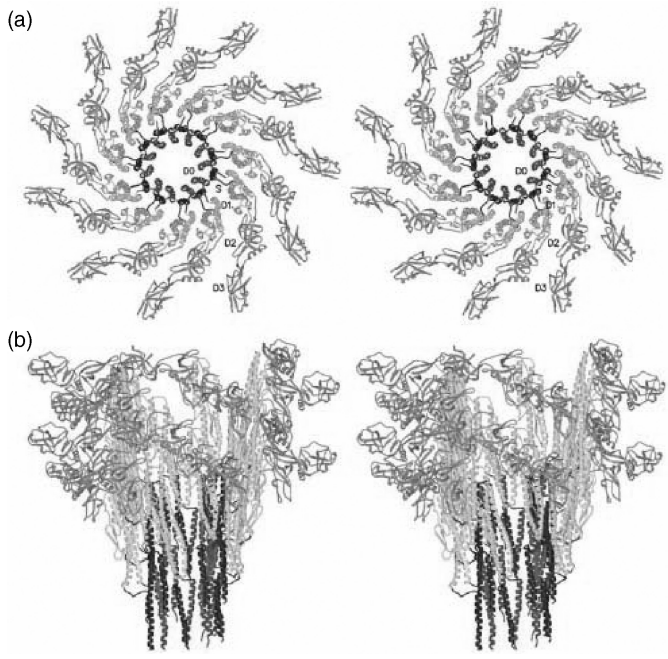

Figure 2.6 Illustration of a helical structure, the bacterial flagellar filament, determined at 4 Å resolution. Stereo views of the ribbon C_α backbone of the filament: (a) end-on view from the distal end of the filament with 11 subunits displayed; and (b) side view with three protofilaments removed for clarity. [Reproduced from Yonekura, K. *et al.* (2003) *Nature* **424**: 643–650]

be shifted by an integer number of unit cells. This is equivalent to describing a helix as being generated by the rotation of an element by a fixed angle α around an axis (the helical axis) in combination with a fixed translation in a direction parallel to that axis. This operation is repeated many times to generate the helix, in the manner of a crystallographic 'screw-symmetry' operator. Nature uses many helical structures, for example, cytoskeletol proteins such as collagen, actin and microtubules, phage particles whose tails have helical organization, bacterial flagella and amyloid fibrils which are associated with a range of human disorders including Alzheimer's disease. Near-atomic resolution has been achieved for the acetyl choline receptor with visualization of beta-sheets and for the R-type flagellar filament (Figure 2.6).

The analysis of *icosahedral structures* now routinely reaches 10 Å resolution and in the better cases is approaching the level achieved for 2D crystals and helical assemblies. This is, in part, due to the 60-fold redundancy of information, which means that each single particle image is equivalent to 60 particles with no symmetry. At the present time good results (6–8 Å) have been achieved for rice dwarf virus, hepatitis B virus and reovirus (Figure 2.7), enabling alpha helices to be traced.

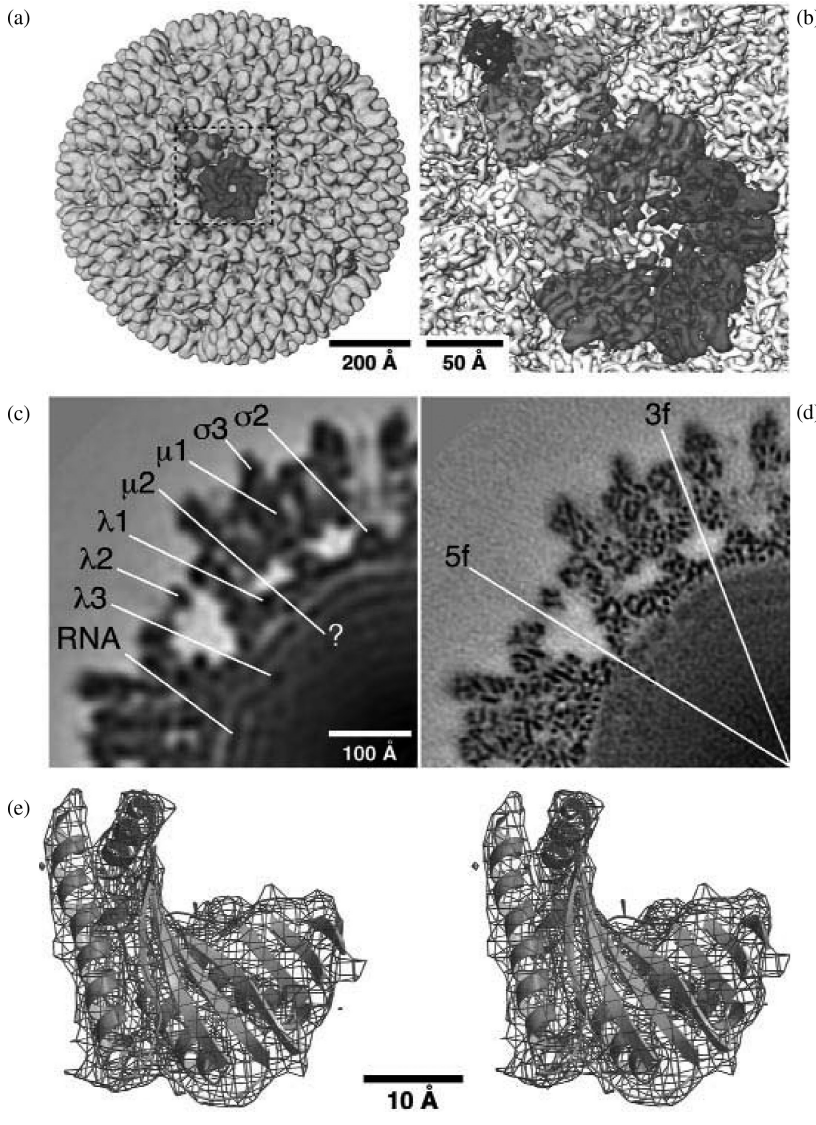

Figure 2.7 Example of single particle reconstruction with icosahedral symmetry at 7.6 Å resolution. Reovirus is shown in both surface-shaded and density section representation and known X-ray structures are docked into the virion. The structure is shown (a) surface-shaded at 20 Å resolution viewed down a 5-fold axis of symmetry. The $\lambda 2$ pentamer (blue) and a $\mu 1_3 \sigma 3_3$ heterohexamer ($\mu 1$, green; $\sigma 3$, red) are highlighted. (b) The outlined region of (a) at 7.6 Å resolution showing finer details with rod-like regions and the interlocking of the 5 λ2 subunits. (c) The approximate location of the viral components in an equatorial density section 2.2 Å thick from the 20 Å rendering; (d) the same as (c) but from the 7.6 Å rendering with locations of 5-fold and 3-fold symmetry axes. Numerous punctate features arise from α-helices viewed end-on. (e) A stereo view of a small portion of the $\lambda 2$ X-ray ribbon structure fitted into the 7.6 Å EM map represented by the wire cage. α-Helices are shown in green and β-strands in yellow. [Reproduced from Zhang, X. *et al.* (2003) *Nat Struct Biol* **10**: 1011–1018]

2.8.3 Single particles with low symmetry

Protein complexes come in all sizes and symmetries. Spliceosomes and ribosomes, with molecular weights in the MDa range, are amongst the larger structures to have been analysed, the smaller are sub-complexes of spliceosomes, the transferrin complex and geminin with molecular weights in the 100 kDa range. Haemocyanines, helicases, portal proteins and heat shock proteins are in-between the two extremes: some of them have cyclical, others tetrameric or other symmetries (Figure 2.8). Each was analysed using the single particle approach. Orientational parameters were determined by projection matching or angular reconstitution. The structures determined for the ribosome, spliceosome and Gro-El (H. Saibil) are in the range 7–9 Å (Figures 2.10 and 2.11). For smaller molecules, cryo-data of the human transferrin receptor–transferrin complex (260 kDa) were analysed at ∼11 Å and human geminin (105 kDa) was analysed in negative stain at ∼17 Å resolution.

2.8.4 Cellular tomography

Recently a number of publications has demonstrated the feasibility of cryo-electron tomography (using an energy filter) to investigate larger, intact structures, such as the complete Herpes Simplex Virus (see Figure 2.12) and a small eukaryotic cell.

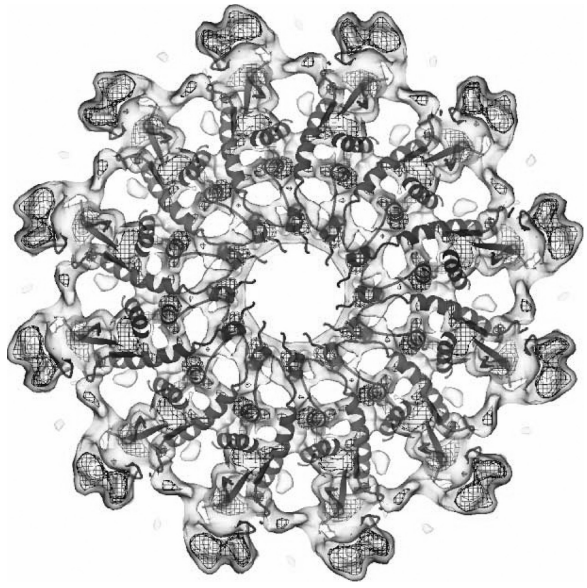

Figure 2.8 Cross-section of the connector of the SPP1 bacteriophage. The connector is a complex of the portal protein and two-head completion proteins. (courtesy of Dr. Orlova) The section shows the X-ray structure of the portal protein fitted into a cryo-EM map. The X-ray structure has been modified from 13-mer into 12-mer, because the connector within the bacteriophage capsid has 12-fold symmetry whereas the portal protein before incorporation into the procapsid has 13-fold symmetry. The excellent fit of density confirms the 10 Å resolution of the EM map

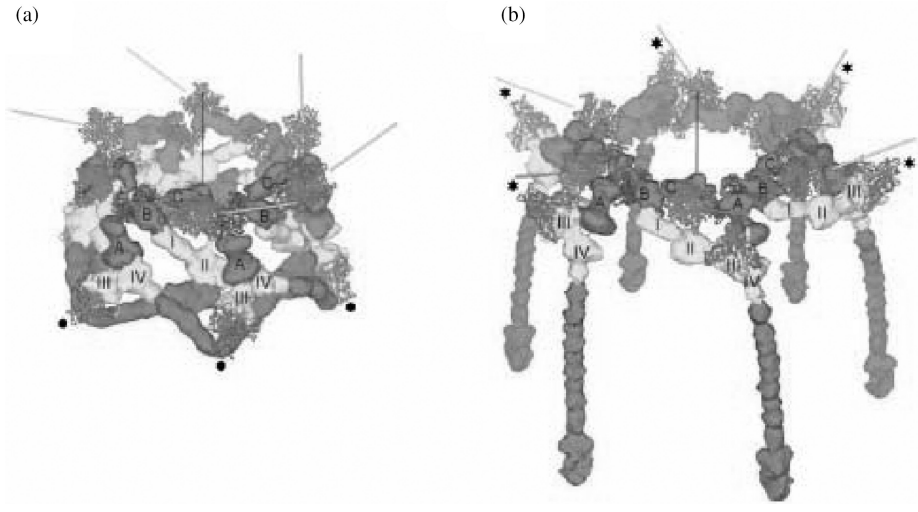

Figure 2.9 Illustration of conformational switching in the contraction of the tail of T4 phage when the baseplate switches from a hexagonal to a star conformation. (a) Structure of the periphery of the baseplate in the hexagonal conformation and (b) in the star conformation. Different proteins are identified by colour: gp7, red; gp8, blue; gp9, green; gp10, yellow; gp11, cyan; gp12, magenta. Combination of cryo-EM at 17 Å resolution and X-ray diffraction. [Reproduced from Leiman, P.G. *et al.* (2004) *Cell* **118**, 419–429]

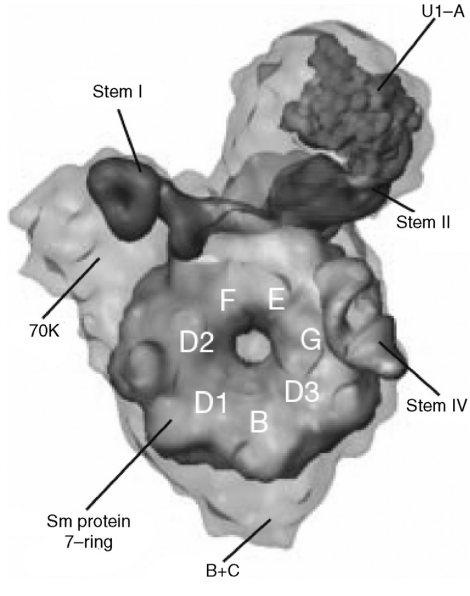

Figure 2.10 Three-dimensional structure of human spliceosomal U1 snRNP at 10 Å resolution. Tentative assignment of domains based on biochemical and structural information. The positions of the Sm proteins are indicated by a yellow ring. [Reproduced from Stark, H. *et al.* (2001) *Nature* **409**: 539–542]

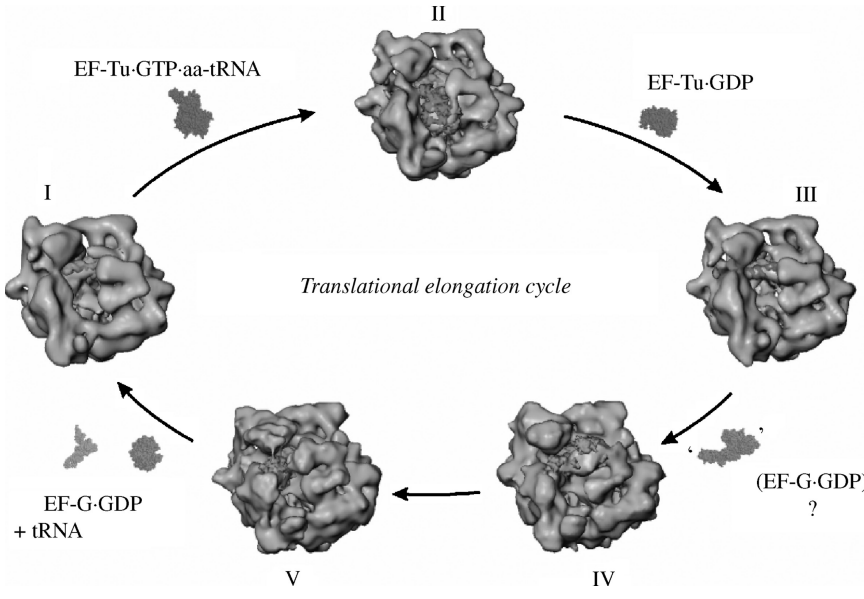

Figure 2.11 Illustration of single particle analysis of various states associated with the elongation cycle of the 70S *E*. coli ribosome (10–15 Å). EM data are shown in gold and other colours are docked X-ray structures of tRNA and various factors. [Reproduced from van Heel, M. *et al.* (2000) *Q. Rev. Biophys.* **33**: 307–369]

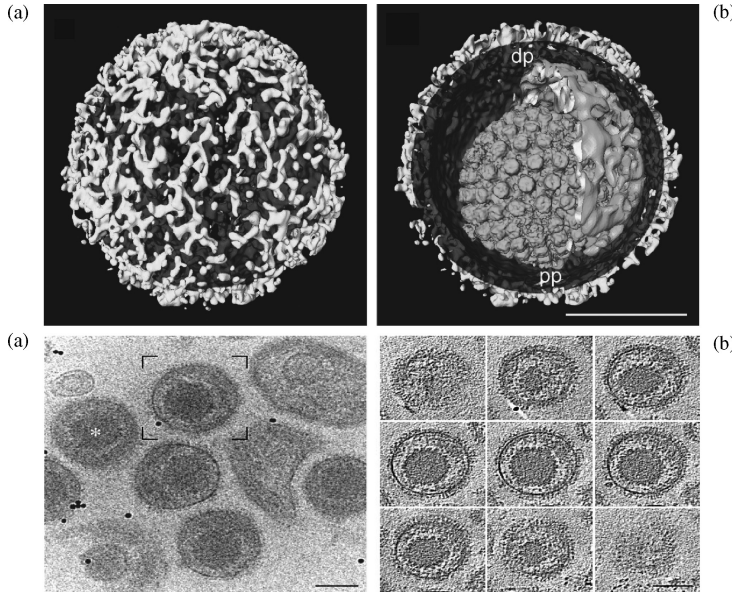

Figure 2.12 Illustration of a tomographic reconstruction of Herpes Simplex Virus. Upper panel: surface-shaded single virion tomogram; left, outer surface showing glycoprotein spikes (yellow) protruding through the membrane (blue) and, right, cutaway view showing the icosahedral capsid (light blue), the tegument (orange) and the envelope with spike proteins (blue and yellow). Lower panel: (a) untilted projected structure and (b) a series of slices through the particle boxed in (a). [Reproduced from Grunewald, K. *et al.* (2003) *Science* **302**: 1396–1398]

Although the resolution is limited to ~50 Å, this represents an exciting step towards systems biology with the visualization of smaller molecules such as the proteasome and Gro EL directly within the cell.

2.9 Conclusions

In the last decade the technique of Cryo-EM combined with image analysis has become a widespread and very powerful tool with which to examine biological structures close to their native state, approaching atomic resolution. Furthermore it enables molecules to be studied in a variety of different functional states using tiny amounts of material. In larger complexes linkages and active sites maybe precisely located in conjunction with ancillary X-ray or NMR data.

The ability to examine whole cells that is emerging with tomographic analysis is bringing the dream of understanding the dynamics of cells in terms of the function and localisation of proteins, their complexes and their relationship to organelles a step closer. Proteomics and systems biology are here with electron microscopy.

Acknowledgement

We thank Dr. Sarah Daniell for help with the bibliography and figures.

Further reading

Steven A.C. (1997). Overview of Macromolecular electron microscopy: an essential tool in protein structural analysis. *Current Protocols in Protein Science*. 17.2.1–17.2.29.

Baker T.S., Olson N.H., and Fuller S.D. (1999). Adding the third dimension to virus life cycles: three-dimensional reconstruction of icosahedral viruses from cryo-electron micrographs. *Microbiology and Molecular Biology Reviews*. 862–922.

Hayat, M.A. (1986). Basic techniques for transmission electron microscopy. Academic Press, N.Y.

Hawkes, P.W. (1972). Electron Optics and Electron Microscopy, Taylor and Francis: London.

Hawkes, P.W. (2004). Advances in Imaging and Electron Physics. Academic Press: London.

Herman, G.T. (1980). Image Reconstruction from Projections – the Fundamentals of Computerized. Tomography. Academic Press: London.

Henderson, R. (1995). The potential and limitations of neutrons, electrons and X-rays for atomic resolution microscopy of unstained biological molecules. *Q. Rev. Biophys*. **28**, 171–193.

Dubochet, J., Adrian, M., Chang, J.-J., Homo, J.-C., Lepault, J., McDowall, A.W., and Schultz, P. (1988). Cryo-electron microscopy of vitrified specimens. *Quat. Rev. Biophys.* **21**, 129–228

Fernandez-Moran, H. (1985). Advances in Electronics and Electron Physics, Vol. **16**, pp. 167–223. Academic Press: London.

Frank, J. (1992). Electron tomography: three-dimensional imaging with transmission electron microscope. Plenum Press. New-York.

Frank, J. (1996). Three-dimensional electron microscopy of macromolecular assemblies. Academic Press. San Diego.

Frank, J. (2002). Single particle imaging of macromolecules by cryo-electron microscopy. *Annu. Rev. Biomol. Struct.* **31**, 303–319.

Moody, M.F. (1990). Electron microscopy of biological macromolecules. In Biophysical Electron Microscopy: Basic concepts and modern techniques (P.W. Hawkes and U.Valdre, eds.) Academic Press, New-York.

Crowther, R.A. (1971). Procedures for three-dimensional reconstruction of spherical viruses by Fourier synthesis from electron micrographs. *Phil. Trans. R. Soc. Lond. B.* 261, 221–230.

Crowther, R.A. & Amos, L. A. (1971). Harmonic analysis of electron images with rotational symmetry. *J. Molec. Biol.* **60**, 123–130.

Fuller, S.D., Butcher, S.J., Cheng, R.H., and Baker T.S. (1996). Three-dimensional reconstruction of icosahedral particles – The uncommon line. *J. Structural Biol.* **116**, 48–55.

Radermacher, M. (1988). Three-dimensional reconstruction of single particles from random and non-random tilt series. *J. Elec. Microsc. Tech.* **9**, 354–394.

Parsons, D.F. (1970). Some Biological Techniques in Electron Microscopy, Parsons, D.F., ed., pp. 1–68. Academic Press: London.

Reimer, L. (1997). Transmission Electron Microscopy – Physics Of Image Formation and Microanalysis. Springer: Berlin.

van Heel M, Gowen B, Matadeen R, Orlova EV, Finn R, Pape T, Cohen D, Stark H, Schmidt R, Schatz M, Patwardhan A. (2000). Single-particle electron cryo-microscopy: towards atomic resolution. *Q. Rev. Biophys.* **33**(4), 307–369.